Biosensors and Bioelectronics 141 (2019) 111442

Contents lists available at ScienceDirect

Biosensors and Bioelectronics

journal homepage: www.elsevier.com/locate/bios

Detecting acid phosphatase enzymatic activity with phenol as a chemical exchange saturation transfer magnetic resonance imaging contrast agent (PhenolCEST MRI)

Jia Zhang[a], Yue Yuan[a,b], Zheng Han[a], Yuguo Li[a], Peter C.M. van Zijl[a,c], Xing Yang[d], Jeff W.M. Bulte[a,b,c], Guanshu Liu[a,c,*]

[a] The Russell H. Morgan Department of Radiology and Radiological Science, Division of MR Research, The Johns Hopkins University School of Medicine, Baltimore, MD, United States
[b] Institute for Cell Engineering, The Johns Hopkins University School of Medicine, Baltimore, MD, United States
[c] F.M. Kirby Research Center for Functional Brain Imaging, Kennedy Krieger Institute, Baltimore, MD, United States
[d] Department of Nuclear Medicine, Peking University First Hospital, Beijing, China

ARTICLE INFO

Keywords:
Acid phosphatase
Phenol
CEST MRI
Enzyme
Biosensor
Prostate cells

ABSTRACT

Phenol contains an exchangeable hydroxyl proton resonant at 4.8 ppm from the resonance frequency of water in the ^{1}H nuclear magnetic resonance (^{1}H NMR) spectrum, enabling itself to be detected at sub-mM concentration by either chemical exchange saturation transfer magnetic resonance imaging (CEST MRI) or exchange-based T_2 relaxation enhancement (T_{2ex}) effect under acidic and basic conditions, respectively. We recently investigated the T_{2ex} effects of phenol and its derivatives, but the CEST characteristics of phenols are unknown in detail, and no study on using the natural CEST MRI effects of phenol for detecting enzymatic activity has been conducted. Herein, on the basis of the inherent CEST MR property of phenol, namely phenolCEST, we developed the first MRI approach to detect acid phosphatase (AcP) enzymatic activity. Upon the activity of AcP at pH = 5.0, non-CEST-detectable enzyme substrate phenyl phosphate was converted to CEST-detectable phenol, providing a simple way to quantify AcP activity directly without the need for a second signalling probe. We showed the application of this phenolCEST biosensor for measuring AcP activity in both enzyme solutions and cell lysates of prostate cells. This work opens a door for the utilization of phenolCEST MRI technique in sensor design and development.

1. Introduction

Acid phosphatases (AcPs) are a family of enzymes that are commonly found in plants and human tissues, like platelets, liver, and prostate (Bull et al., 2002). Of these, prostatic acid phosphatase (PAcP) is over 100 times more abundant than AcPs in other tissue types (Heller, 1987). PAcP was used as a clinical biomarker for prostate cancer long before the discovery of prostate specific membrane antigen, but some studies re-assessed its value to be a prognostic indicator for intermediate- or high-risk prostate cancer (Dattoli et al., 1999; Saito et al., 2007; Taira et al., 2007). The human PAcP gene encodes for three protein isoforms, i.e. cellular PAcP, secretory PAcP, and transmembrane PAcP (Muniyan et al., 2014). The clinical assay for AcP in serum relies on the level of secretory PAcP. Recently, methods for AcP detection are developed on the basis of colorimetry and fluorometry due to high sensitivity and low cost (Deng et al., 2017; Guo et al., 2013; Huang et al., 2016; Lu et al., 2007; Qian et al., 2015; Sun et al., 2015; Xie et al., 2012; Xu et al., 2014). Among these, the Kind-King method is the most widely used one, which indirectly detects the converted phenol from substrate phenyl phosphate using a chromogenic reaction (Kolliopoulos et al., 2015). On the other hand, however, we noticed that a unique magnetic resonance imaging (MRI) method was developed for the detection of alkaline phosphatase (ALP) at pH = 7.4 with the use of fosfosal (a phosphorylated form of salicylic acid) (Daryaei et al., 2016). This approach, namely CatalyCEST, adopts a relatively new MRI technique that detects the activity of an enzyme by observing the changes in the chemical exchange saturation transfer (CEST) signal as the result of the change in the chemical structure of a CEST biosensor catalyzed by the enzyme (Hingorani et al., 2013; Sinharay et al. 2016, 2018).

* Corresponding author. The Russell H. Morgan Department of Radiology and Radiological Science, Division of MR Research, The Johns Hopkins University School of Medicine, Baltimore, MD, United States.
E-mail address: guanshu@mri.jhu.edu (G. Liu).

https://doi.org/10.1016/j.bios.2019.111442
Received 16 April 2019; Received in revised form 10 June 2019; Accepted 14 June 2019
Available online 20 June 2019
0956-5663/

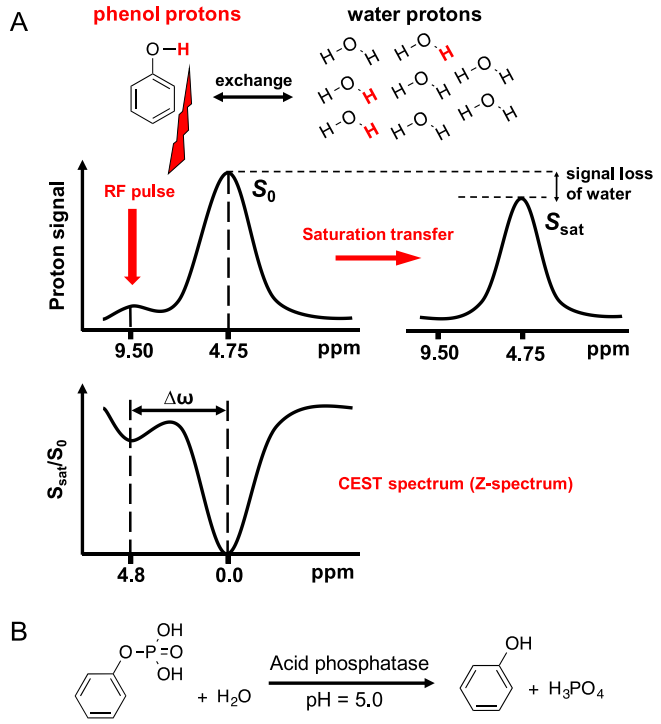

Fig. 1. (A) Principles for the chemical exchange saturation transfer using phenol as the model molecule. The phenolic hydroxyl proton is selectively saturated at its resonance frequency by RF pulse, and this magnetization saturation is transferred to water protons repetitively, resulting in the visible loss of water signal in the proton spectrum. Saturation is normalized (S_{sat}/S_0) as a function of irradiation frequency, generating a so-called CEST spectrum (or Z-spectrum). Direct water saturation at 4.75 ppm causes the disappearance of the signal, and this frequency is assigned to 0 ppm in Z-spectra (Modified from (van Zijl and Yadav, 2011). (B) Acid phosphatase catalyzes the hydrolysis of phenyl phosphate to release the phosphate group and phenol under acidic pH.

CEST MRI is an imaging method that relies on direct chemical exchange of protons with bulk water. A number of small molecules possessing protons that exchange rapidly with surrounding water protons has been developed as CEST MRI contrast agents (Cai et al., 2012; Chan et al., 2012; Li et al., 2016; Liu et al., 2016a; Longo et al., 2011; Ryoo et al., 2017; Yang et al., 2013). The CEST contrast mechanism involves selective irradiation of those exchangeable protons at their resonance frequencies using a radiofrequency (RF) saturation pulse, which after repetitive exchange of the saturated protons with fresh water protons on the MR time scale (at several seconds), reduces the MRI signal of water consequently (Fig. 1A). This loss of bulk water signal is typically demonstrated by a CEST spectrum (or Z-spectrum), and the frequency corresponding to the water protons at 4.75 ppm is assigned to 0 ppm in Z-spectra. To quantify the CEST effect, the asymmetric magnetization transfer ratio ($MTR_{asym} = S_{sat}^{-\Delta\omega}/S_0 - S_{sat}^{+\Delta\omega}/S_0$) is used (van Zijl and Yadav, 2011). One of the most remarkable features for CEST MRI is that it can be used to detect diamagnetic molecules at sub-mM concentrations without the need for metal labelling.

Phenol is an important building block molecule to the syntheses of many biologically active compounds. We recently showed that phenol and its derivatives could be directly detected through the inherently carried exchangeable hydroxyl protons, depending on pH and temperature, either via enhancement of transverse relaxation rate (T_2) due to -OH exchange or CEST MRI (Zhang et al., 2018b). In particular, the phenolic hydroxyl proton has a chemical shift 4.8 ppm apart from the resonance frequency of water (Fig. S1). When pH ≥ 6.5, the phenolic proton exchange rate surpasses the slow-to-intermediate regime needed for CEST contrast, while it generates a detectable decrease in water T_2 relaxation time (known as the T_{2ex} effect) (Aime et al., 2005; Soesbe et al., 2011; Yadav et al., 2014). The exchange rate slows down at lower pH (i.e., pH ≤ 6.0), allowing the detection of phenol by CEST MRI. Given the optimal pH for AcP to function is at pH = 5.0-5.3 (Kruzel and Morawiecka, 1982), we hypothesized that the inherent CEST signal of phenol could be used to determine the activity of AcP under acidic conditions by using phenyl phosphate as the probe (Fig. 1B).

2. Experimental section

2.1. Chemicals

Acid phosphatase from potato (P3752, 0.5 ~ 3 units/mg), alkaline phosphatase from porcine kidney (P4439, 100 unit), and sodium phenyl phosphate dibasic dihydrate (P7751) were purchased from Sigma (St. Louis, MO, USA). Phenol and disodium 4-nitrophenyl phosphate were purchased from Combi-Blocks (San Diego, CA, USA). Unless otherwise specified, all reagents were of analytical grade and used directly without purification.

2.2. CEST MRI

All sample were loaded into 1 mm-diameter glass capillaries and then placed in a customized holder for MRI measurements on a 9.4 T Bruker Avance system equipped with a 20 mm birdcage RF coil. All measurements were performed at 37 °C. CEST-weighted images were acquired using a modified single slice rapid acquisition with relaxation enhancement (RARE) sequence as described previously (Liu et al., 2017), with B_1 = 5.9 μT, t_{sat} = 4 s, TR = 6 s, effective TE = 43.2 ms, RARE factor = 32, slice thickness = 2 mm, matrix size = 64 × 64, resolution = 0.25 × 0.25 mm^2, and two averages. To obtain the Z-spectra, the saturation offsets of CEST-weighted images were swept from -6 to 6 ppm at an increment of 0.2 ppm around the water resonance (0 ppm). The absolute water resonant frequency shift was measured using a WAter Saturation Shift Reference (WASSR) method modified with Lorentzian analysis (Liu et al., 2013).

Data processing was performed using custom-written scripts in MATLAB (Mathworks, Waltham, MA). MTR_{asym} was used to quantify the CEST signal by removing direct saturation effects from the acquired Z-spectrum that are assumed to be symmetric with respect to the water resonance frequency. MTR_{asym} is defined as $MTR_{asym} = (S_{sat}^{-\Delta\omega} - S_{sat}^{+\Delta\omega})/S_0$, where $S_{sat}[-\Delta\omega, +\Delta\omega]$ is the water signal intensity in the presence of a saturation pulse at frequency offsets ± Δω, and S_0 is water signal intensity in the absence of a saturation pulse.

2.3. Estimation of exchange rate of the phenolic hydroxyl proton

The exchange rate of the phenolic hydroxyl proton at pH = 5.0 was measured using the modified QUantifying Exchange using Saturation Time (QUEST) method (Liu et al., 2011; McMahon et al., 2006). In brief, the CEST contrast for 20 mM phenol was measured with saturation delays of 0.5, 1, 2, 3, 4, and 5 s, using a saturation field strength of 5.9 μT and a repetition time set to 10 s, based on the RARE imaging sequence described above. Calculated MTR_{asym} values were then fitted using numerical solutions to the Bloch-McConnel equations with an exchange rate (k_{ex}) as the unknown. The water T_1 and T_2 values were experimentally determined using the RARE-based saturation recovery sequence and the CPMG multi-echo spin echo sequence, respectively (Zhang et al. 2018a, 2018b).

2.4. Contrast-to-noise ratio (CNR)

The CNR was calculated by using the equation below:

$$CNR = (S_{sample} - S_{buffer}) / \sigma_{buffer}$$

where S_{sample} and S_{buffer} are signal intensities of sample and buffer and

σ_{buffer} is the standard deviation of signal intensity of buffer.

2.5. Analysis of enzyme kinetics

At 37 °C in acetate buffer (pH 5.0, 10 mM, containing 10 mM Mg^{2+}), 0.1 mg/mL of AcP (molecular mass: 69 kDa) was incubated with increasing concentrations of phenyl phosphate (PP) ranging from 2 to 15 mM for 5 min. The reaction was halted by freezing the samples, after which CEST MRI was measured at pH = 5.0 and 37 °C, using a 5.9 μT/4 s RF saturation pulse. We assumed that the conversion of PP was linearly correlated with time over this time frame. The correlation of reaction velocity with the concentration of substrate can be fitted by the Michaelis-Menten model, based on which the Michaelis constant (K_M) and the maximum rate (V_{max}) were obtained. The k_{cat} was calculated from the V_{max}/[AcP], where [AcP] was measured to be 1.5 μM.

2.6. Quantification of AcP enzyme concentration in cell lysates by the standard addition method

Human prostate cell lines including normal RWPE-1 and cancerous DU 145 were purchased from the American Type Culture Collection (Rockville, MD, USA). RWPE-1 cells were cultured in Keratinocyte Serum Free Medium (KSFM) containing 0.05 mg/mL bovine pituitary extract and 5 ng/mL epidermal growth factor. DU 145 cells were cultured in Eagle's Minimum Essential Medium (EMEM) containing 10% fetal bovine serum and penicillin–streptomycin. 1×10^6 cells were treated with 0.1 mL of lysis solution (mammalian protein extraction reagent, mPER, Thermo Scientific), and stored at 4 °C for 1 h. Afterwards, the pH of solution was titrated to 5.0, and the insoluble debris was cleared through centrifugation, leaving AcP enzyme in the supernatant. For the standard addition method, each 10 mM PP was mixed with cell lysate (15 μL for RWPE-1 and 10 μL for DU 145), cell lysate + 0.015 mg mL^{-1} AcP, and cell lysate + 0.03 mg mL^{-1} AcP in acetate buffer (pH = 5.0, final volume: 400 μL) and incubated at 37 °C for 1 h, followed by CEST measurement at 37 °C and pH = 5.0, using a 5.9 μT/4 s RF saturation pulse. Cell lysate alone in acetate buffer was used as control. For the quantification, ΔMTR_{asym} was used and defined as MTR_{asym}(cell lysate + PP) – MTR_{asym}(cell lysate) or MTR_{asym}(cell lysate + AcP + PP) – MTR_{asym}(cell lysate).

3. Results and discussion

3.1. Characterization of phenolCEST for assessing AcP activity

We first characterized the CEST contrast signal of phenol (phenolCEST) at 37 °C and pH = 5.0 in 10 mM acetate buffer at 9.4 T magnetic field strength. A well-defined CEST peak was observed at 4.8 ppm (Fig. 2A), with proton exchange rate estimated to be 940 Hz using the QUEST method (Fig. S2). This rate is below the chemical shift difference at 9.4 T ($\Delta\omega$ = 1920 Hz), placing it in the slow exchange MR regime and making phenol suited for CEST imaging at this acidic pH. In fact, the phenolCEST signal kept almost the same at pH between 5.0 and 6.0 at 37 °C (Fig. S3). The magnitude of CEST contrast for 10 mM phenol was measured to be 11.3 ± 0.1% using a 5.9 μT/4 s continuous wave (CW) RF pulse. Given the concentration of water protons is about 110 M, CEST MRI provides an amplification of the NMR signal of phenol proton by > 1,200 times (110 M × 0.113/10 mM = 1243). The amplitude of CEST contrast depended strongly on the saturation power (B_1) of the RF pulse, increasing steadily with the B_1 from 1.2 to 5.9 μT, where a plateau was attained (Fig. 2B). At B_1 = 5.9 μT, we measured the CEST contrast of phenol as a function of concentration from 2 to 10 mM. As shown in Fig. 2C, we obtained a good linear correlation of the CEST signal with phenol concentration (R^2 = 0.998), thereby allowing the use of CEST measures to determine concentration of phenol by the following equation: C_{phenol}(mM) = MTR_{asym}(4.8 ppm)%/1.143. Under the present conditions, 2 mM phenol produced a CEST contrast of 2.4% and a contrast-to-noise ratio (CNR) of 27, implying a sub-mM detectability for the in vitro studies.

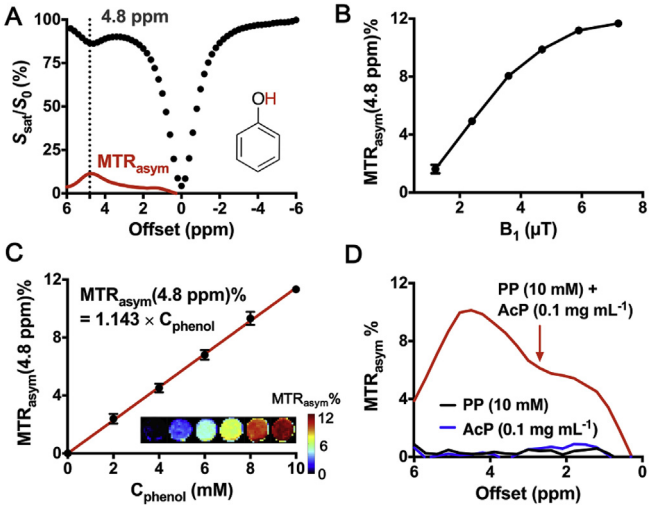

Fig. 2. Characterization of phenolCEST in the detection of acid phosphatase activity in 10 mM acetate buffer at pH_{CEST} = 5.0 and 37 °C (B_0 = 9.4 T). (A) Z-spectrum and corresponding MTR_{asym} spectrum of 10 mM phenol. (B) MTR_{asym} contrast at 4.8 ppm for 10 mM phenol as a function of saturation power (B_1), using a saturation time of 4 s. (C) MTR_{asym} contrast at 4.8 ppm for different concentrations of phenol and the fitted calibration curve. The inset shows the pseudo-colored MTR_{asym} map at 4.8 ppm, with phenol concentration at 0, 2, 4, 6, 8, and 10 mM, respectively, from left to right. (D) MTR_{asym} spectra of PP (10 mM), AcP (0.1 mg mL^{-1}), and the solution after enzymatic reaction for 1 h. Note: for figures A, C, and D, a 5.9 μT/4 s RF saturation pulse was used; for figures B and C, data are shown as mean ± SD (n = 3).

To make use of the phenolCEST to detect AcP activity, we incubated 10 mM phenyl phosphate (PP) with 0.1 mg mL^{-1} of AcP in acetate buffer (10 mM, pH_{reac} = 5.0, containing 10 mM $MgCl_2$ to stimulate AcP activity) at 37 °C for 1 h. Immediately after reaction, the samples were transferred to capillaries (Liu et al., 2010) and measured for the CEST MRI signal at the same conditions (pH_{CEST} = 5.0 and 37 °C). There are two pH conditions in the measurement. To minimize the confusion, we define the pH for the enzymatic reaction as pH_{reac}, and the pH for CEST measurement as pH_{CEST}. As shown in Fig. 2D, neither the substrate nor the enzyme alone showed an appreciable CEST signal. In contrast, the incubated sample exhibited a strong CEST signal peaked at 4.8 ppm (MTR_{asym} = 10%), corresponding to 8.7 mM phenol that was produced.

3.2. Optimization of parameters to detect AcP activity by phenolCEST: effect of enzymatic reaction time and pH_{reac}

We then studied the enzyme kinetics of AcP using phenolCEST. We measured the dynamic CEST signals of 10 mM PP + AcP in the presence of three individual enzyme concentrations from 5 min to 4 h. At each time point, solutions were immediately transferred from water bath to refrigerator to retard the enzymatic reaction. The CEST signals of all samples were then measured at pH_{CEST} = 5.0 ± 0.1 and 37 °C using a 5.9 μT/4 s RF saturation pulse. Fig. 3A shows noticeable CEST contrast of phenol as early as 5 min even for 0.025 mg mL^{-1} of enzyme. The generated contrasts correlated positively with the enzyme concentration, attaining 60% (0.025 mg mL^{-1}), 74% (0.05 mg mL^{-1}), and 82% (0.1 mg mL^{-1}), respectively, after reaction for 1 h relative to the values obtained at 4 h. The most rapid kinetic changes were observed within the first 5 min for all three enzyme concentrations, and correlated with the enzyme concentration positively. The concentration of converted phenol at each time point could be calculated using the calibration curve of phenol (Fig. 2C) in order to provide an estimate of the conversion ratio, as shown in Fig. 3B. It shows that 6.8%, 23%, and

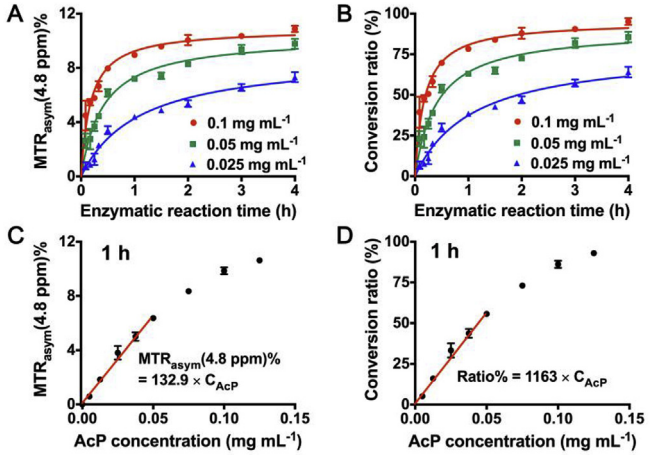

Fig. 3. Quantification of AcP activity by phenolCEST in 10 mM acetate buffer at pH_{CEST} = 5.0 and 37 °C, using a 5.9 μT/4 s RF saturation pulse (B_0 = 9.4 T). (A) CEST contrast and (B) the corresponding enzymatic conversion ratio of 10 mM PP incubated with different enzyme concentrations as a function of time. The data were non-linearly fitted. (C) CEST contrast and (D) the corresponding enzymatic conversion ratio of 10 mM PP incubated with different enzyme concentrations after reaction for 1 h. Both data were linearly fitted from 0 to 0.05 mg mL^{-1} of enzyme. Data are shown as mean ± SD (n = 3).

39% of PP was converted to phenol within the first 5 min, respectively, with respect to the enzyme concentration of 0.025, 0.05, and 0.1 mg mL^{-1}, and after reaction for 1 h, the corresponding conversion ratios turned to 38%, 63%, and 78%. This indicates the conversion of PP increased by 5.6-fold, 2.7-fold, and 2-fold, respectively, for 1 h of reaction compared to 5 min with respect to 0.025, 0.05, and 0.1 mg mL^{-1} of enzyme. Hence prolonging time of reaction is more useful to enhance the enzymatic conversion at a lower enzyme concentration. By means of the initial reaction velocity during the first 5 min of reaction at the use of 0.1 mg mL^{-1} enzyme, we performed a Michaelis-Menten kinetic analysis, with the kinetic parameters estimated to be: K_M = 3.5 mM; $V_{max} = 1.2 \times 10^{-2}$ mM s^{-1}; k_{cat} = 8.1 s^{-1}; and k_{cat}/K_M (catalytic efficiency) = 2.3 mM^{-1} s^{-1} (Fig. S4). This K_M value for PP is larger than the value (1.25 mM) reported for *p*-nitrophenyl phosphate (Kruzel and Morawiecka, 1982) in agreement with the fact that the latter has more affinity for AcP than PP (Cosnier et al., 2006).

We also found that solution pH_{reac} under which the enzymatic reaction occurred could affect the phenolCEST signal, which decreased gradually with pH_{reac} increasing from 5.0 to 7.4 (Fig. S5). To demonstrate the use of phenolCEST MRI to quantify AcP activity, we mixed 10 mM PP with different amounts of AcP (0.005, 0.0125, 0.025, 0.0375, 0.05, 0.075, 0.1, and 0.125 mg mL^{-1}) for 1 h at pH_{reac} = 5.0 and 37 °C. Fig. 3C-D show that increasing the enzyme concentration leads to a proportionally increased MTR_{asym} signal and enlarged enzymatic conversion ratio. Specifically, the CEST contrast or the conversion ratio increased linearly with enzyme concentration till 0.05 mg mL^{-1}. The minimal enzyme concentration to cause significant phenolCEST contrast change (CNR > 5) for 1 h of reaction was estimated to be 5 μg mL^{-1} or 2.5 ~ 15 units/L. It should be noted that the limit of detection may vary with the reaction time, with a higher threshold by shorter incubation, and vice versa.

Table 1 shows a list of methods recently developed for the detection of AcP, which are based on fluorometry or colorimetry. Compared to these methods, our method has a relatively low sensitivity due to the inherently less sensitive nature of CEST MRI than fluorometry or colorimetry (by 3 orders). However, despite the low sensitivity, CEST MRI is a high-resolution imaging strategy that can be used to detect AcP activity in heterogeneous samples, which is challenging to be pursued by other avenues. The acquisition time of the MRI method is also longer than those of optical methods, which however may be improved by using ultrafast CEST methods (Ryoo et al., 2017; Xu et al., 2016). However, the assay itself typically takes 30-60 min for sufficient enzyme reaction, which is the limiting factor for the total assay time. Hence, the detection time should not be considered as a major disadvantage of the MRI method. In contrast to more than half of the previous methods with decreasing signal change as the readout, our method employs the appearance of CEST signal, changing from "OFF state" to "ON state", which is advantageous because it normally produces higher contrast (Guo et al., 2018; Xie et al., 2012; Xu et al., 2014; Zhang and Yang, 2013). The most remarkable advantage of this biosensor is that the CEST signal is generated by the enzyme product directly and hence only one component (substrate) is needed. In contrast, all the previous biosensors require at least the addition of two components (i.e., enzymatic substrate and signaling probe). Therefore, it demonstrates a prototype approach for detecting AcP, which can be tailored (by using different substrates) to other types of phosphatases, especially those that can be used as drug targets, such as tartrate-resistant AcP (Honig et al., 2006) and tyrosine phosphatase (Hoekstra et al., 2016). This is challenging for methods based on fluorometry or colorimetry.

3.3. Assessing AcP activity in prostate cells by phenolCEST and selectivity test

We applied the biosensor to detect AcP levels in prostate cell lysates to show that this phenolCEST technique can tolerate biologically relevant components. Cellular AcP is located within endosome-like vesicles and lysosomes, where acidic pH (5.0-5.5) is favored for the enzyme activity (Quintero et al., 2007; Zhou et al., 2012). Here we compared the expression levels of AcP in two cell lines, i.e., normal prostate RWPE-1 cells and prostate cancerous DU 145 cells, quantified by using the standard addition method. We found that the mammalian protein extraction reagent used for lysis of cells barely affected the catalysis of AcP or the phenolCEST signal intensity (Fig. S6). As shown in Fig. 4A-B, for both cell lysates, mixing lysate with PP caused the phenolCEST signals increase, and the further addition of known concentrations of AcP, the signals more enhanced. Then the original AcP concentrations were determined by the x-intercept values of the extrapolated plots of the phenolCEST contrast measured at different amounts of AcP added to the cell lysates (Fig. 4C). Our results (Fig. 4D) showed that a significantly higher level of AcP was present in DU 145 cell line (48 ± 5 μg/10^6 cells) than in RWPE-1 cell line (20 ± 2.5 μg/10^6 cells). Given the possible difference of specific activity between the potato-derived AcP and the mammalian cellular AcP, it may be better to show that the level of AcP in DU 145 cells was estimated to be 0.024 ~ 0.144 units/10^6 cells, compared to 0.01 ~ 0.06 units/10^6 cells in RWPE-1 cells. Under the present conditions, the limit of detection for the enzyme was 2.5 ~ 15 units/L (vide supra). Based on the estimation that per 10^6 cells the concentrations of AcP were 240 ~ 1440 units/L for DU145 and 100 ~ 600 units/L for RWPE-1, the detection limit of cells was measured to be 1.8×10^4 in order to differentiate the two cell types by this biosensor.

The major interference in the AcP assay is definitely from ALP, another common enzyme with the same function as AcP but preferably active under basic pH (Liu et al., 2016b; Sun et al., 2018). To demonstrate that the contribution of ALP is negligible at the present acidic condition, we incubated 10 mM PP with 2 units of ALP at pH_{reac} = 5.0 and pH_{reac} = 10.0 for 4 h at 37 °C. Afterwards, both solutions were titrated to pH_{CEST} = 5.0 and measured for their phenolCEST signals. It showed that ALP was only functional at pH_{reac} = 10 but not at pH_{reac} = 5.0 (Fig. S7), indicating a good selectivity of this biosensor for AcP. Recently, biosensors relying on salicylic acid (SA)-based CEST MRI have been developed to detect a variety of enzymes, including ALP (Daryaei et al., 2016). However, the CEST signal from the SA proton decreases in intensity with acidifying pH (Sinharay et al., 2017; Yang et al., 2013), and thus limiting its application for the detection of AcP as

Table 1
A list of recently developed methods for the detection of AcP in terms of sensitivity, time for detection, and signal readout. [a]Here shows the components on which the biosensors are developed; [b]here shows the dynamic detection range and limit of detection. The unit is generalized as U/L, in which U is the abbreviated form of unit for specific activity of enzyme.

Method[a]	Sensitivity[b]	Time for detection	Signal change	Reference
PPE4 + /pNPP	0.3-6 U/L (0.05 U/L)	> 60 min	Increasing	Xie et al. (2012)
SQ/$(NaPO_3)_6$	0.35-35 U/L (0.35 U/L)	> 40 min	Increasing	Xu et al. (2014)
$CuInS_2$ QDs/Cu^{2+}/ATP	6.4-192 μU/L (3.1 μU/L)	> 40 min	Decreasing	Lin et al. (2015)
AuNCs/Fe^{3+}/PPi	0.1-3 U/L (0.1 U/L)	> 15 min	Decreasing	Sun et al. (2015)
CQDs/Ni^{2+}/PPi	18.2-1300 U/L (5.5 U/L)	> 60 min	Decreasing	Qian et al. (2015)
GQDs/PDDA/$(NaPO_3)_6$	30-420 μU/L (12 μU/L)	> 40 min	Decreasing	Na et al. (2016)
CuNCs/pNPP	3.8-22.8 U/L (1.3 U/L)	> 32 min	Decreasing	Huang et al. (2016)
Ch-PtNPs/TMB/AAP	0.25-2.5 U/L (0.016 U/L)	> 35 min	Decreasing	Deng et al. (2017)
NH_2-MIL-101/OPD/H_2O_2/PPi	0.01-30 U/L (0.005 U/L)	> 80 min	Increasing	Li et al. (2019)
Phenyl phosphate	5-50 U/L (5 U/L)	> 60 min	Increasing	Our work

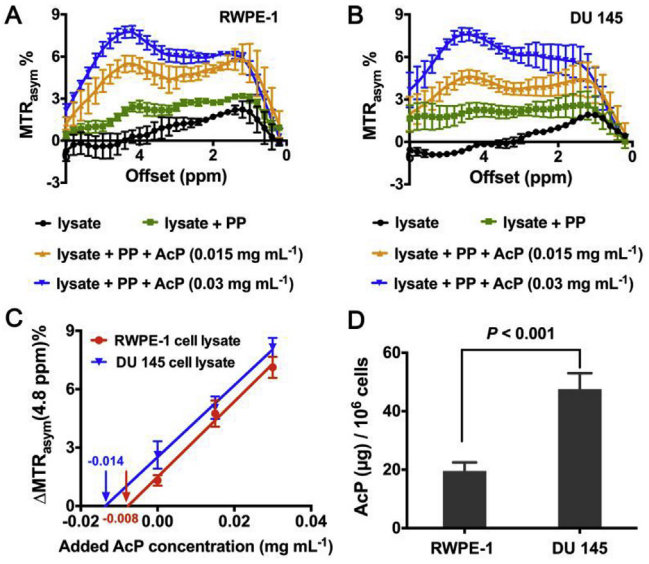

Fig. 4. Measurement of AcP levels in prostate RWPE-1 cell lysates and prostate cancerous DU 145 cell lysates at pH_{CEST} = 5.0 and 37 °C, using a 5.9 μT/4 s RF saturation pulse (B_0 = 9.4 T). (A, B) The MTR_{asym} spectra for lysates alone, lysates + PP (10 mM), lysates + PP (10 mM) + AcP (0.015 mg mL^{-1}), and lysates + PP (10 mM) + AcP (0.03 mg mL^{-1}). (C) Correlation of ΔMTR_{asym}(4.8 ppm)% with added AcP concentration. Marked are the *x*-intercept values of the extrapolated plots, from which the unknown concentrations of AcP in cell lysates can be quantified. (D) Amount of AcP per 1 million cells for both cell lines ($P < 0.001$, two-tailed unpaired Student's *t*-test). Data are shown as mean ± SD (n = 3).

performed by phenolCEST MRI. The novelty of this work is that it demonstrates the use of CEST MRI to detect enzymatic activity at acidic pH, whereas most CEST biosensors are performed at neutral pH. Taken together, these results demonstrated the feasibility of phenolCEST MRI for determining the enzymatic activity of AcP in biological samples.

4. Conclusions

In summary, we presented a novel CEST MRI method to detect phenol under acidic pH, simply by its exchangeable phenol proton resonant at 4.8 ppm. This method, called phenolCEST, was utilized to develop an imaging approach to detect AcP enzymatic activity at acidic pH and demonstrated on both enzyme solutions and prostate cell lysates. Despite of several drawbacks such as low sensitivity and potential cytotoxicity of phenol, which limit the immediate in vivo application, the proposed method has a number of unbeatable features compared to previous fluorometry- or colorimetry-based approaches. In future work, we will improve the biocompatibility of this method by using less toxic phenol derivatives as CEST probe, such as catechol (Szydlowska et al., 2006), which expands the scope of exchangeable protons for developing bioorganic CEST MRI biosensors under acidic pH.

Declaration of interests

There are no conflicts to declare.

CRediT authorship contribution statement

Jia Zhang: Conceptualization, Data curation, Formal analysis, Validation, Writing - original draft, Writing - review & editing. **Yue Yuan:** Data curation, Formal analysis, Validation, Writing - review & editing. **Zheng Han:** Formal analysis, Software, Validation, Writing - review & editing. **Yuguo Li:** Data curation, Writing - review & editing. **Peter C.M. van Zijl:** Validation, Funding acquisition, Writing - review & editing. **Xing Yang:** Conceptualization, Writing - original draft, Writing - review & editing. **Jeff W.M. Bulte:** Validation, Writing - review & editing. **Guanshu Liu:** Conceptualization, Formal analysis, Funding acquisition, Project administration, Software, Supervision, Writing - review & editing.

Acknowledgements

This work was supported by NIH grants R03EB021573, R01CA211087, R21CA215860 (G.L.), and R01EB015032 (P.C.M.v.Z.).

Appendix A. Supplementary data

Supplementary data to this article can be found online at https://doi.org/10.1016/j.bios.2019.111442.

References

Aime, S., Calabi, L., Biondi, L., De Miranda, M., Ghelli, S., Paleari, L., Rebaudengo, C., Terreno, E., 2005. Magn. Reson. Med. 53, 830–834.
Bull, H., Murray, P.G., Thomas, D., Fraser, A.M., Nelson, P.N., 2002. Mol. Pathol. 55, 65–72.
Cai, K.J., Haris, M., Singh, A., Kogan, F., Greenberg, J.H., Hariharan, H., Detre, J.A., Reddy, R., 2012. Nat. Med. 18, 302–306.
Chan, K.W.Y., McMahon, M.T., Kato, Y., Liu, G.S., Bulte, J.W.M., Bhujwalla, Z.M., Artemov, D., van Zijl, P.C.M., 2012. Magn. Reson. Med. 68, 1764–1773.
Cosnier, S., Mousty, C., Cui, X., Yang, X., Dong, S., 2006. Anal. Chem. 78, 4985–4989.
Daryaei, I., Ghaffari, M.M., Jones, K.M., Pagel, M.D., 2016. ACS Sens. 1, 857–861.
Dattoli, M., Wallner, K., True, L., Sorace, R., Koval, J., Cash, J., Acosta, R., Biswas, M., Binder, M., Sullivan, B., Lastarria, E., Kirwan, N., Stein, D., 1999. Int. J. Radiat. Oncol. Biol. Phys. 45, 853–856.
Deng, H.H., Lin, X.L., Liu, Y.H., Li, K.L., Zhuang, Q.Q., Peng, H.P., Liu, A.L., Xia, X.H., Chen, W., 2017. Nanoscale 9, 10292–10300.
Guo, J.J., Gao, M.X., Song, Y.L., Lin, L., Zhao, K.F., Pan, T., Liu, D., Zhu, Z., Yang, C.Y.J., 2018. Front Chem 6, 618.
Guo, P., Yan, S., Zhou, Y., Wang, C., Xu, X., Weng, X., Zhou, X., 2013. Analyst 138, 3365–3367.
Heller, J.E., 1987. J. Urol. 137, 1091–1103.
Hingorani, D.V., Randtke, E.A., Pagel, M.D., 2013. J. Am. Chem. Soc. 135, 6396–6398.
Hoekstra, E., Peppelenbosch, M.P., Fuhler, G.M., 2016. Cancer Res. 76, 193–196.

Honig, A., Rieger, L., Kapp, M., Krockenberger, M., Eck, M., Dietl, J., Kammerer, U., 2006. BMC Canc. 6, 199.
Huang, Y.Y., Feng, H., Liu, W.D., Zhou, Y.Y., Tang, C., Ao, H., Zhao, M.Z., Chen, G.L., Chen, J.R., Qian, Z.S., 2016. Anal. Chem. 88, 11575–11583.
Kolliopoulos, A.V., Kampouris, D.K., Banks, C.E., 2015. Analyst 140, 3244–3250.
Kruzel, M., Morawiecka, B., 1982. Acta Biochim. Pol. 29, 321–330.
Li, S., Hu, X., Chen, Q., Zhang, X., Chai, H., Huang, Y., 2019. Biosens. Bioelectron. 137, 133–139.
Li, Y., Chen, H., Xu, J., Yadav, N.N., Chan, K.W., Luo, L., McMahon, M.T., Vogelstein, B., van Zijl, P.C., Zhou, S., Liu, G., 2016. Oncotarget 7, 6369–6378.
Lin, Z.H., Liu, Z.P., Zhang, H., Su, X.G., 2015. Analyst 140, 1629–1636.
Liu, G., Gilad, A.A., Bulte, J.W., van Zijl, P.C., McMahon, M.T., 2010. Contrast Media Mol. Imaging 5, 162–170.
Liu, G., Song, X., Chan, K.W., McMahon, M.T., 2013. NMR Biomed. 26, 810–828.
Liu, G.S., Banerjee, S.R., Yang, X., Yadav, N., Lisok, A., Jablonska, A., Xu, J.D., Li, Y.G., Pomper, M.G., van Zijl, P., 2017. Nat Biomed Eng 1, 977–982.
Liu, G.S., Liang, Y.J., Bar-Shir, A., Chan, K.W.Y., Galpoththawela, C.S., Bernard, S.M., Tse, T., Yadav, N.N., Walczak, P., McMahon, M.T., Bulte, J.W.M., van Zijl, P.C.M., Gilad, A.A., 2011. J. Am. Chem. Soc. 133, 16326–16329.
Liu, H., Jablonska, A., Li, Y., Cao, S., Liu, D., Chen, H., Van Zijl, P.C., Bulte, J.W., Janowski, M., Walczak, P., Liu, G., 2016a. Theranostics 6, 1588–1600.
Liu, X.G., Xing, X.J., Li, B., Guo, Y.M., Zhang, Y.Z., Yang, Y., Zhang, L.F., 2016b. Biosens. Bioelectron. 81, 460–464.
Longo, D.L., Dastru, W., Digilio, G., Keupp, J., Langereis, S., Lanzardo, S., Prestigio, S., Steinbach, O., Terreno, E., Uggeri, F., Aime, S., 2011. Magn. Reson. Med. 65, 202–211.
Lu, J.C., Fang, C., Xu, H.R., Huang, Y.F., Lu, N.Q., 2007. Clin. Chim. Acta 375, 76–81.
McMahon, M.T., Gilad, A.A., Zhou, J.Y., Sun, P.Z., Bulte, J.W.M., van Zijl, P.C.M., 2006. Magn. Reson. Med. 55, 836–847.
Muniyan, S., Ingersoll, M.A., Batra, S.K., Lin, M.F., 2014. Biochim. Biophys. Acta 1846, 88–98.
Na, W.D., Hu, T.Y., Su, X.G., 2016. Analyst 141, 4926–4932.
Qian, Z., Chai, L., Zhou, Q., Huang, Y., Tang, C., Chen, J., Feng, H., 2015. Anal. Chem. 87, 7332–7339.
Quintero, I.B., Araujo, C.L., Pulkka, A.E., Wirkkala, R.S., Herrala, A.M., Eskelinen, E.L., Jokitalo, E., Hellstrom, P.A., Tuominen, H.J., Hirvikoski, P.P., Vihko, P.T., 2007. Cancer Res. 67, 6549–6554.
Ryoo, D., Xu, X., Li, Y.G., Tang, J.A., Zhang, J., van Zijl, P.C.M., Liu, G.S., 2017. Anal. Chem. 89, 7758–7764.
Saito, T., Hara, N., Kitamura, Y., Komatsubara, S., 2007. Urology 70, 702–705.
Sinharay, S., Fernandez-Cuervo, G., Acfalle, J.P., Pagel, M.D., 2016. Chem. Eur J. 22, 6491–6495.
Sinharay, S., Randtke, E.A., Howison, C.M., Ignatenko, N.A., Pagel, M.D., 2018. Mol. Imaging Biol. 20, 240–248.
Sinharay, S., Randtke, E.A., Jones, K.M., Howison, C.M., Chambers, S.K., Kobayashi, H., Pagel, M.D., 2017. Magn. Reson. Med. 77, 2005–2014.
Soesbe, T.C., Merritt, M.E., Green, K.N., Rojas-Quijano, F.A., Sherry, A.D., 2011. Magn. Reson. Med. 66, 1697–1703.
Sun, J., Yang, F., Yang, X.R., 2015. Nanoscale 7, 16372–16380.
Sun, J., Zhao, J.H., Bao, X.F., Wang, Q.F., Yang, X.R., 2018. Anal. Chem. 90, 6339–6345.
Szydlowska, D., Campas, M., Marty, J.L., Trojanowicz, M., 2006. Sensor. Actuator. B Chem. 113, 787–796.
Taira, A., Merrick, G., Wallner, K., Dattoli, M., 2007. Oncology (Williston Park) 21, 1003–1010.
van Zijl, P.C.M., Yadav, N.N., 2011. Magn. Reson. Med. 65, 927–948.
Xie, Y.H., Tan, Y., Liu, R.X., Zhao, R., Tan, C.Y., Jiang, Y.Y., 2012. ACS Appl. Mater. Interfaces 4, 3784–3787.
Xu, X., Yadav, N.N., Song, X.L., McMahon, M.T., Jerschow, A., van Zijl, P.C.M., Xu, J.D., 2016. J. Magn. Reson. 265, 224–229.
Xu, Y.Q., Li, B.H., Xiao, L.L., Ouyang, J., Sun, S.G., Pang, Y., 2014. Chem. Commun. 50, 8677–8680.
Yadav, N.N., Xu, J.D., Bar-Shir, A., Qin, Q., Chan, K.W.Y., Grgac, K., Li, W.B., McMahon, M.T., van Zijl, P.C.M., 2014. Magn. Reson. Med. 72, 823–828.
Yang, X., Song, X.L., Li, Y.G., Liu, G.S., Banerjee, S.R., Pomper, M.G., McMahon, M.T., 2013. Angew. Chem. Int. Ed. 52, 8116–8119.
Zhang, J., Han, Z., Lu, J.Q., Li, Y.G., Liao, X.H., van Zijl, P.C., Yang, X., Liu, G.S., 2018a. Chem. Eur J. 24, 15013–15018.
Zhang, J., Li, Y.G., Slania, S., Yadav, N.N., Liu, J., Wang, R.F., Zhang, J.H., Pomper, M.G., van Zijl, P.C., Yang, X., Liu, G.S., 2018b. Chem. Eur J. 24, 1259–1263.
Zhang, J., Yang, X.R., 2013. Analyst 138, 434–437.
Zhou, K.J., Liu, H.M., Zhang, S.R., Huang, X.N., Wang, Y.G., Huang, G., Sumer, B.D., Gao, J.M., 2012. J. Am. Chem. Soc. 134, 7803–7811.